Recent Advances in Aerospace Hydraulics, November 24–25, 1998, Toulouse, France

A UNIFIED CONTROL STRATEGY FOR FLIGHT CONTROL ACTUATORS

KLIFFKEN Markus Gustav
Robert Bosch GmbH
Dept. K4/EKE4
P.O. Box 1163
D-77830 Buehlertal
Phone +49 (0) 7223 82-2644
Email: Markus.Kliffken@pcm.bosch.com

GOJNY Marcus Heinrich
Technical University of Hamburg–Harburg
Section Aircraft Systems Engineering (2-08)
D-21071 Hamburg
Phone +49 (0) 40 74315-211
Fax: +49 (0) 40 74315-270
Email: gojny@tu-harburg.de

ABSTRACT

Analyzing the structure of an aircraft's electrohydraulic actuation system, the traditional realization of the closed–loop system shows a considerable limitation of dynamics. Enhanced control concepts like state control enable a remarkable improvement. Gradually, the outlined descriptive design procedure leads to a robust sampled–data controller, which automatically manages the parameter uncertainties and finite word-length effects, occuring in low hardware performances or with rapid sampling. These considerations are verified by extensive simulations and real tests. Finally, a conceivable application is presented regarding to the interaction of actuator dynamics and the flexible structure of an airfoil.

KEYWORDS

Primary Flight Control System, Hydraulic Actuator, Sampled Data Control, Robust Control, Parameter Space Design, Delta-Transformation, Aeroservoelasticity.

I INTRODUCTION

Due to high power density, control surfaces of modern commercial and military aircraft are driven by hydraulic linear actuators. In current Fly–by–Wire systems the flight control computers contain digital controllers, signalling the electrohydraulic servo drives. Due to the changing flight operation conditions and natural aging, the physical parameters vary considerably. Although the complete system is characterized by high order, drastic nonlinearities and significant parameter uncertainties, a low order linear position controller is aspired. Therefore the classical third, respectively fourth order system description of a hydraulic actuator can simply be adapted to a linear Multi–Model–System. Nowadays, low performance specification justifies the application of traditional proportional control, which shows sufficient dynamics in most cases. In future projects, e.g. very large aircraft with extremely flexible structures, the need for improved dynamics becomes obvious.

II SYSTEM DESCRIPTION

Commonly, the control surfaces of civil transport aircraft are actuated by two parallel electrohydraulic servo drives. While one operates in status active, the second represents not only cold stand–by, but significantly, contributes to systems damping. Further details describe e.g. [2, 5, 13, 14]. Fig. 1 sketches

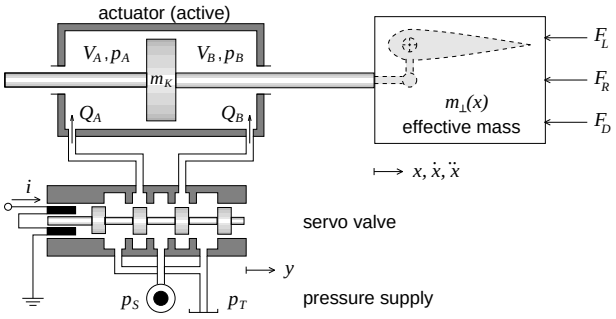

Figure 1: Simplified actuation system

the simplified model of such an actuation system, which is quite similar to standard servo actuation. It consists of an actuator and a servo valve, latter connected to the constant pressure supply $p_V = p_S - p_T$. The displacement of the actuator piston x is forced by the pressure drop $\Delta p = p_A - p_B$, due to the controlled flows through the valve $Q_{A,B}$, adjusted by the current i.

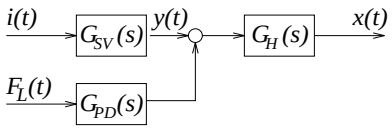

Figure 2: Linear model structure

The actuator fastenings to the wing box and to the control surface lead to a nonlinear kinematic and result in the variable mass $m_\perp$, which is affected by the forces of the damping actuator F_D, friction F_F and external aerodynamic loads F_L. Altogether, this description yields a system of three differential equations

$$\begin{aligned} C_H\,\Delta\dot{p} &= Q - A\dot{x} \\ m_\perp\,\ddot{x} &= A\,\Delta p - F \\ \tau_{SV}\,\dot{y} + y &= i\,, \end{aligned} \tag{1}$$

with an algebraic equation determining the flow through the servo valve

$$Q_A = Q_B \approx Q = B_{SV}\,y\,\sqrt{|p_V - \Delta p\,\mathrm{sign}(y)|/2}\,. \tag{2}$$

Considering (1), C_H represents the position depending hydraulic capacity, A the piston area, $F = F_L + F_D + F_F$ the sum of forces and τ_{SV} the decay factor of the servo valve.

Usually, the nonlinear model (1) is linearized at the operation point ($\Delta p = 0$, $x = 0$, $\dot{x} = 0$ and $y = 0$). Thereby the linear state space model leads to the more illustrative set of transfer functions (Fig. 2). Herein

$$G_H(s) = \frac{X(s)}{Y(s)} = \frac{k_H\,\omega_H^2}{s\,(s^2 + 2\,d_H\,\omega_H\,s + \omega_H^2)} \tag{3}$$

describes the interaction between actuator and valve position and

$$G_{SV} = \frac{Y(s)}{I(s)} = \frac{k_{SV}}{\tau_{SV}\,s + 1} \tag{4}$$

the reaction of the valve position to the input current. The effect of aerodynamic loads on the system is characterized by

$$G_F(s) = \frac{X(s)}{F_L(s)} = \underbrace{k_F\,(\tau_H\,s - 1)}_{=\;G_{PD}(s)}\,G_H(s)\,. \tag{5}$$

Real flight conditions and systems nonlinearities entail varying physical parameters. Assuming the mentioned linear model, the hydraulic damping and eigenfrequency can be isolated as the two dominant uncertain parameters [7, 8]. Both span the uncertainty domain Q, which is normally fixed as a rectangular box. To avoid unnecessary conservative assumptions in control design, the real set should be considered instead (Fig. 3). The two boundary parameter combinations $\mathbf{q}^\perp = [\omega_H^\perp \;\; d_H^+]^\mathrm{T}$ and $\mathbf{q}^+ = [\omega_H^+ \;\; d_H^\perp]^\mathrm{T}$ as well as the nominal operation point $\mathbf{q}^0 = [\omega_H^0 \;\; d_H^0]^\mathrm{T}$ are used in further discussion.

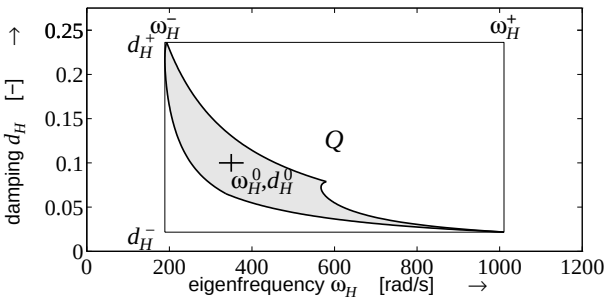

Figure 3: Parameter space

III COMMON CONTROL

Due to the dominant integral system dynamics of hydraulic actuators, a proportional feedback controller

$$k_x = \frac{\omega_B}{k_H} \tag{6}$$

adjusts the specified bandwidth ω_B. Maintaining simplicity, the servo valve dynamics are neglected ($G_{SV}(s) = k_{SV}$). The stability bound follows from Eq. (3) applying Hurwitz criterion

$$k_x < \frac{2\,d_H\,\omega_H}{k_H\,k_{SV}}\,. \tag{7}$$

Considering the weak damping of the hydraulic actuation system (see Fig. 3), this result is only of theoretical meaning. Actually, the adjusted bandwidth and hydraulic eigenfrequency has to be situated apart from each other for more than a decade to obtain a step response free of oszillation $\omega_B \ll \omega_H$. Therefore, a strong limitation of the reachable bandwidth is manifested by proportional feedback. With regard to the magnitude plot of the closed–loop system, the gap between the amplitude at the natural frequency and the 0 dB–line

$$\Delta A = \frac{\omega_B}{2\,d_H\,\omega_H - \omega_B} \tag{8}$$

contains more descriptive information. That value is suitable to quantify the residual ripple of the step response (Fig. 4). Moreover, it reveals a close relationship to the infinity norm of the sensitivity function

$$||S(\mathrm{j}\omega)||_\infty \approx 1 + \Delta A\,. \tag{9}$$

A substantial increase of the closed–loop system dynamics will be enabled by introducing auxiliary feedback variables

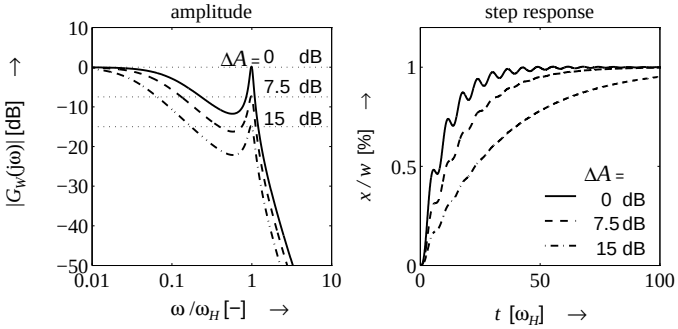

Figure 4: Closed loop dynamics

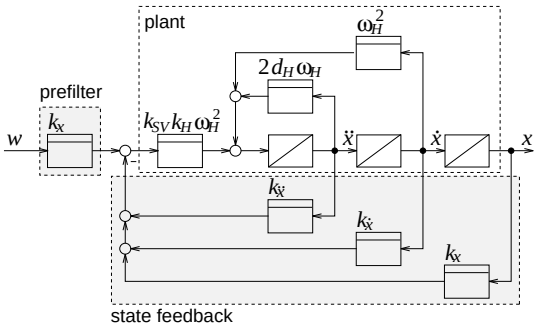

Figure 5: State–space control

(Fig. 5). Unfortunately the pressure drop feedback causes a systematic steady–state error in the presence of external loads ($F_L \neq 0$). Replacing it by the acceleration feedback generates more convenient steady-state properties. Resuming the neglect of the servo valve dynamics to perform stability analysis, the Hurwitz criterion yields

$$0 < k_x < \omega_H^2\, k_{\ddot{x}} \quad \text{and} \quad k_{\ddot{x}} > 0\,. \tag{10}$$

Obviously, the necessary condition to guarantee systems stability consists of the acceleration feedback gain. Tuning the velocity feedback gain $k_{\dot{x}}$ only effects additional damping. Furthermore, applying describing function method [4] shows, that these conditions guarantee freedom from limit cycles, which could have occured due to the saturation of the servo valve flows. The Second Rule of Robustness [1] outlines a guide for convenient pole placement (Fig. 6). The pole at the origin of coordinates has to be shifted along the real axis into the left half-plane ($s_0 = 0 \rightarrow -\omega_B$) to adjust the specified bandwidth. Regarding the demanded damping D, the conjugate-complex poles $s_{1,2}$ are displaced at the arc with the constant radius $r = \omega_H$. Assuming a simple first–order system to estimate servo valve dynamics, the corresponding pole $s_3 = -1/\tau_{SV}$ is fixed, because that placement shows sufficient dynamics and do not influence the system characteristics. Finally, the procedure leads to the typical Winschegradski pole configuration

$$s_0 = -\lambda,\; s_{1,2} = (-1 \pm \mathrm{j})\,\lambda \quad \text{and} \quad s_3 = -1/\tau_{SV} \tag{11}$$

and verifies that a state space controller could increase the possible performance to the maximum bandwidth for an

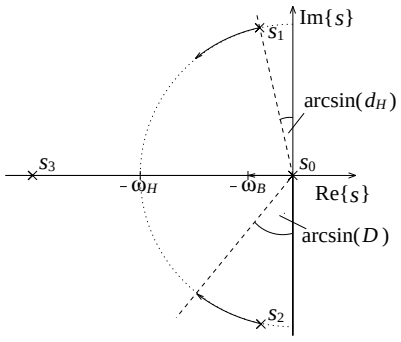

Figure 6: Pole placement

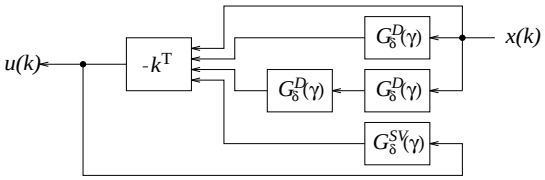

Figure 7: Dynamic controller

oscillation-free step response

$$\omega_B^+ = \frac{\omega_H}{\sqrt{2}}\,. \tag{12}$$

Compared to the classic proportional control, the profit amounts to more than a decade, applying state feedback. Even though all states are measureable, the high effort installing additional redundant sensors can be avoided, if suitable estimates of the velocity, the acceleration and the valve piston stroke are established. In continuous–time control systems a combination of a simple parallel model approximating the servo valve dynamics and a reduced order observer with its two eigenvalues at $\hat{s}_{1,2} = -\omega_H$ could be designed, without limiting the systems stability. In discrete–time control the observer could be better replaced by time invariant differentiation filters [11] (Fig. 7)

$$G_z^D(z) = \frac{4\,z^{\left(\frac{d+1}{2}\right)}}{\pi\,T} \sum_{k=1}^{\left(\frac{d+1}{2}\right)} \frac{-1^{k+1}}{(2\,k-1)^2}\,(z^k - z^{1\perp k})\,. \tag{13}$$

IV ADVANCED CONTROL STRATEGY

Sampled–Data System Description

Taking the most favoured controller implementation within the flight control computer into consideration, the design of a sampled-data controller is of primary interest. That requires an implementation with robust numerical properties such as less sensitivity to finite–wordlength effects. Hence, the use of the Delta–Transformation [12] ensures those demands. Furthermore, the continuity between discrete– and continuous–time system description is recovered. Automatically, the sampled–data controller and the continuous–time counterpart converge by increasing the sampling rate ($T \longrightarrow 0$). Thus the advantages of quasi–continuous control and digital signal processing can be combined without excessive effort.

The corresponding state–space model yields the well–known structure

$$\begin{aligned} \delta\mathbf{x}(k) &= \mathbf{A}_\delta\,\mathbf{x}(k) + \mathbf{B}_\delta\,\mathbf{u}(k)\,, \quad \mathbf{x}(0) = \mathbf{x}_0 \\ \mathbf{y}(k) &= \mathbf{C}\,\mathbf{x}(k) + \mathbf{D}\,\mathbf{u}(k)\,. \end{aligned} \tag{14}$$

The discrete–time system and input matrices can be derived by utilizing the matrix exponential

$$\mathbf{A}_\delta = \frac{(\mathrm{e}^{\mathbf{A}T} - \mathbf{I})}{T} \;\text{ and }\; \mathbf{B}_\delta = \int_0^T \frac{\mathrm{e}^{\mathbf{A}\tau}}{T}\,d\tau\,\mathbf{B}\,, \tag{15}$$

whereas the output and transit matrices are equal to their continuous–time representatives. Assuming fast sampling, the bilinear equivalents are very often a sufficient approximation

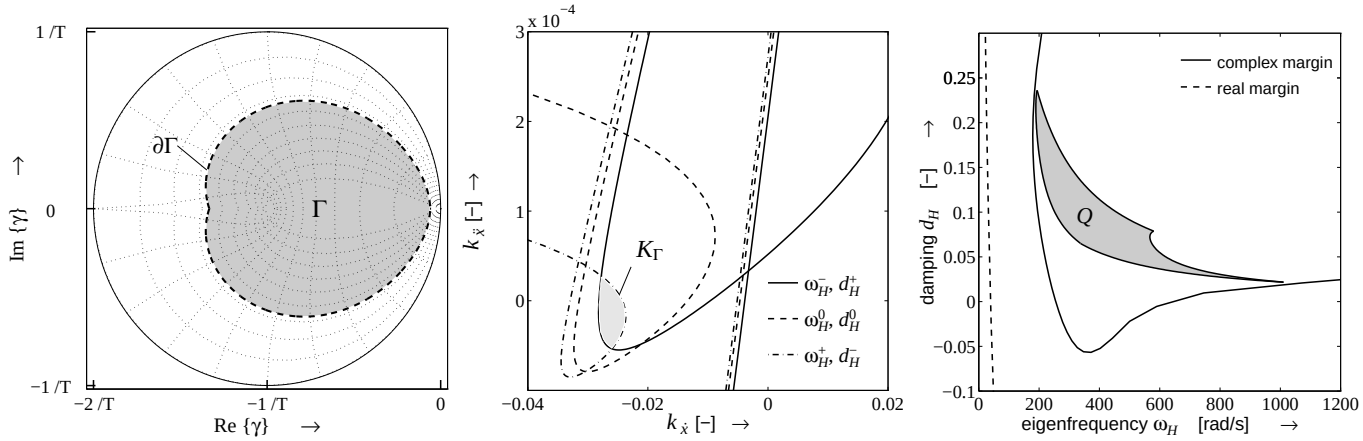

(a) Pole region assignment

(b) Controller plane

(c) Stability margins

Figure 8: Simulaneous Γ-stabilization

and allow the application of algebraic methods. The assigned frequency domain results from the definition of the complex variable of the Delta–Transformation

$$\gamma = \frac{z-1}{T} \ , \tag{16}$$

which must be applied e.g. to the universal formular of the differential filter (13). With regard to the design task at issue and respecting the postulated rapid sampling, a filter of third order shows sufficient properties.

Parameter Space Design Method

Considering the result of the former section, the bandwidth can be increased for more than a decade, applying state–space control. With regard to the considerable parameter uncertainties of the linear model, the use of Parameter Space Design [1] ensures a strict systematic procedure and allows a transparent design of a parametric robust controller

$$\mathbf{k} = \left[\begin{array}{cccc} k_x & k_{\dot{x}} & k_{\ddot{x}} & k_y \end{array} \right]^{\mathrm{T}} . \tag{17}$$

Selecting characteristic operating points yields a corresponding Multi Model Problem which is solved by Simultaneous Γ–Stabilisation, as proceeded in [8, 7].

The significant minimal damping and a tripled bandwidth

$$D^{\perp} = 0.33 \quad \text{and} \quad \omega_B^{\perp} = 2\pi 10 \ . \tag{18}$$

stand for increased performance specifications and illustrate the enhanced demand on actuator dynamics. This design objective yields an assigned pole region Γ in the complex γ–plane, where all closed–loop eigenvalues of the selected repesentatives has to be placed (Fig. 8a). At the first sight the margin ∂Γ reveals a close similarity to an equiangular . However, being reminded of the corresponding continuous–time set Γ [1] nearby the origin, the affinity to a hyperbola can be discovered on closer inspection. In the sequel ∂Γ tends to the curve of constant damping and encloses the admissible pole set.

Generally, two main synthesis steps can be separated, continuing the design procedure:

1. The position feedback gain follows straight from the specified minimal bandwidth, as performed in Eq. (6)

   $$k_x = \frac{1-\exp(-\omega_B^{\perp} T)}{k_{SV}\, k_H\, T} \ . \tag{19}$$

   Moreover, to tune k_x means regulating systems disturbance properties, e.g. the stiffness against external loads, which is very important for the compensation of the systematic hinge moment as well as additional loads.

   After fixing the bandwidth, the obtained pole-zero map reveals a centered root locus of the servo valve model within the specified region Γ. Thus, a feedback of the servo valve piston position y appears to be not necessary

   $$k_y = 0 \ . \tag{20}$$

   Otherwise the servo valve feedback gain could be selected and the position feedback gain corrected by cascade control design technics.

2. A detailed systems analysis enables to reduce the set of free controller parameters successively. Then, the controller synthesis could be resumed by Direct Pole Region Assignment [1]. Transformating the eigenvalue constraints (Fig. 8a) applied to the three representatives of the Multi Model System yields the related subsets of the feedback gains $(k_{\dot{x}}, k_{\ddot{x}})$. The set of feedback gains, which assign the closed–loop system eigenvalues into Γ, follow from the intersection of these subsets

   $$K_{\Gamma} = \bigcap_{j=1}^{N} K_{\Gamma}^{(j)} \ , \qquad N = 3 \ . \tag{21}$$

   Fig. 8b displays the real and complex margins as straight lines and curves. For example, selecting the tuple $(k_{\dot{x}} = -0.026, k_{\ddot{x}} = 5 \cdot 10^{\perp 5})$ at the lower limit of the admissible region, an inverse transformation yields the course

of the stability margins in the uncertain parameter space, considering the just determined controller. This represents a simple possibility to check the effect of the designed controller. Due to the choice of the velocity and acceleration feedback tuple at the intersection of the complex boundaries of the two extrema, $[\omega_H^{\perp},\ d_H^{+}]^{\mathrm{T}}$ and $[\omega_H^{+},\ d_H^{\perp}]^{\mathrm{T}}$, the complex margin of that controlled system touches exactly the uncertainty domain Q (Fig. 8c).

Discovering the axis $k_{\ddot{x}} = 0$ cuts K_Γ, it is even more effective to make the selection out of that set. Thus, the acceleration feedback gain and the servo valve piston position feedback gain could be neglected. This result differs from the robust synthesis of the continuous-time controller, where that feedback represents the decisive one. Even to guarantee more enhanced performance specifications, the avoidance of additional measuring points and sensors is possible. Measuring only x, a complete state feedback is realized by implementing a dynamic controller, consisting of the constant feedback $\mathbf{k}$, a first order parallel model, which estimates the servo valve dynamics, and a network of differentiation filters $G_\delta^D(\gamma)$ to approximate the derivatives of x (Fig. 7).

Validation/Experiments

In order to evaluate the designed sampled–data controller in a real environment, the presented controller structure is implemented on a test bench, which is located at the department Aircraft Systems Engineering of the Technical University of Hamburg–Harburg (Fig. 9). Its structure copies the real configuration of a redundant actuator system, here in particular the inboard aileron of the AIRBUS A340. The inertia of any control surface can be imitated by the exchangeable disk mass, which is mechanically coupled to the two actuators and the dynamic load simulation by a shaft. The imitation of the torsion behavior of the aileron spar as well as the flexible coupling of the actuators to the wing box succeeds by the adjustable fastenings of the outside actuator. In order to draw a comparison to the conventional implementation, the developed control concept is implemented in both of the discrete–time descriptions: z–domain and γ–domain. However the system and controller architecture remains identical. The parameterizing is adapted for the respective sampling instance, following the

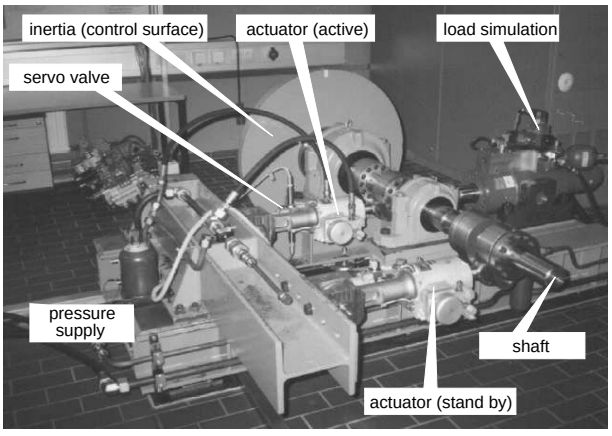

Figure 9: Test bench

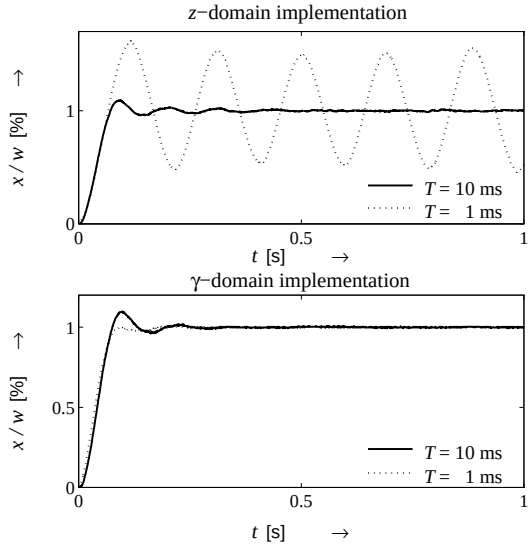

Figure 10: Measured step responses

already mentioned performance specifications: overshoot-free transient response and a bandwidth of $\omega_B = 2\pi 10$ Hz. Illustrating the numerical robustness, a poor resolution of the digital signal processing components has to be adjusted. The resolution of the measuring signal is amounted to 6 bits, which represents a drastic signal quantization. A minimum word length of 8 bits is available for the calculation of the control signal by the dynamic controller. That calculation is carried out by means of floating point arithmetic, whereby the finite word length effects turns out clear, but smaller compared to the fixed point arithmetic of usual micro controllers. Fig. 10 displays the command step response at two different sampling instances. The direct comparison indicates a partly substantial deviation from the design target. Considering the quite large estimated sample period $T = 10$ ms, both implementations show a comparable transient response in accordance with the specified dynamics, approximately. Decreasing the sampling instance to the currently demanded value $T = 1$ ms, however the classic implementation in z–domain starts executing limit cycles. By way of contrast, the performance of the chosen implementation in γ–domain is characterized by smaller post–pulse oscillations already at the long sampling instance. This constantly improves with the decrease of the sampling time. Finally, for $T = 1$ ms almost no increase of the performance is recognizable and the specification is fulfilled exactly. Beyond that, the parametric robustness is proved by validation on the test rig as well as in extensive nonlinear simulation.

V AEROELASTIC INTERACTION

Most recent investigation is done to integrate the actuator dynamics into analysis of aeroelasticity [3]. A first approach consists of the classical two-dimensional model of an airfoil, well–known as the typical section, connected with the comprehensive model of the actuator (Fig. 11). Considering inertia, elastic forces and moments, damping and aerodynamic forces by the assumption of infinitesimal h, α, δ yield the equation of motion. Using unsteady incompressible flow theory, the aero-

dynamic forces result from the separated approach of a noncirculatory and circulatory part, the latter is based on Theodorsen's function [3]. The entire model yields the mechanical subsystem, of which feedback consists of the aerodynamics, causing the systematic, dynamic hinge moment. That couples to the mechanical input and closes the inner loop of the plant. As the result of stability analysis, the systems properties are often represented as damping trajectories of proper motions by the true air speed U

$$d_i(U) = -\mathrm{Re}\{\lambda_i(U)\} \,/\, |\lambda_i(U)| \,,\; i \in [1,2] \,. \qquad (22)$$

Fig. 12 sketches $d_i(U)$ using different actuator controllers. Clearly, it can be detected, that the torsion mode causes the instability of the aeroelastic system, when the trajectory cuts $d = 0$. Moreover, the actuator with state space controller increases the damping of this proper motion substantially. This is enabled by a significant higher forward gain with simultaneous compensation of the disadvantages of a pure proportional controller. Naturally, the flutter boundary is not enlarged by any actuator controller. Due to the substantial interaction between actuator and aeroelastic plant investigations have to begin, concerning the controllability and observability of the aeroelastic eigenvalues. That leads to the feedback of further measuring or estimating signals, if necessary. Therefore, the enhancement of the actuator state controller to an aeroelastic output controller is expected. At present, this is the subject of current research, which includes the extension of the airfoil model and the experimental validation at the institute–own test rig with integrated aeroelastic plant by hardware–in–the–loop simulation.

VI CONCLUDING REMARKS

It has been demonstrated that the nonlinear model of the electrohydraulic actuator with considerable parameter uncertainties led to a linear Multi Model System. Limitations of bandwidth, which occured in connection with a proportional controller, could be recovered by state control. The simultaneous pole region assignment [1] was easily transferred to the used δ-operator system description. In addition to the received enhanced performance, the presented design grants numerical robustness concerning finite word length effects. That led to a general design method, which yielded the continuous-time controller as special case $T \to 0$. The method proposed was experimentally shown to be extremely efficient in implementing controllers with low hardware performances but a high

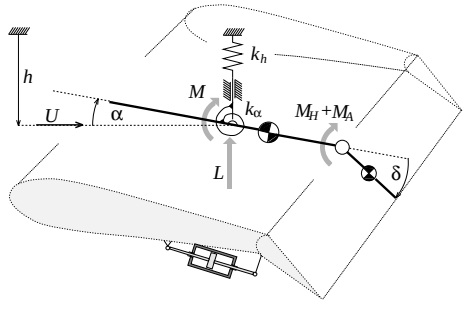

Figure 11: Two-dimensional airfoil with aileron

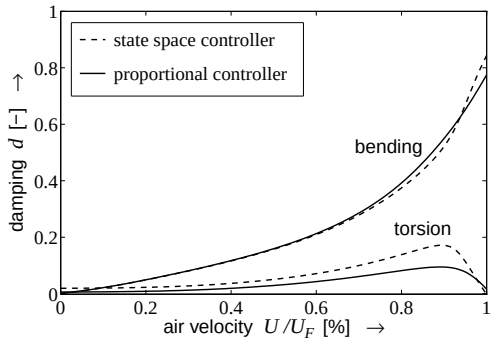

Figure 12: Damping of the airfoils proper motions

sampling rate. The overall observations can be summarized as follows: Applying the outlined method, the obtained sampled-data controller guarantees enhanced robust system properties without spending any additional effort to considerations about implementation effects. This encouraging result motivates further work on influencing interactions between the actuator system and the aeroelastic environment, especially with a more detailed mechanical model and allocated aerodynamics. The ongoing investigations focus on analysing the aeroelastic interaction and outlining a suitable method to design an aeroelastic controller.

REFERENCES

[1] *Ackermann, J.; et. al.*: Robust Control — Systems with Uncertain Physical Parameters. Springer, London, 1993.

[2] *Bossche, D.; et. al.*: Airbus A3330/340 Primary Flight Control Actuation System. SAE Committee A6, Atlanta, 1991.

[3] *Dowell, E.H.(Ed.)*: A Modern Course in Aeroelasticity. Kluwer, Dordrecht, 3rd ed., 1995.

[4] *Gelb, A.; Vander Velde, W.E.*: Multiple–Input Describing Functions and Nonlinear system Design. McGraw Hill, New York, 1968.

[5] *Green, W.L.*: Aircraft Hydraulic Systems. J. Wiley & Sons, Chichester, 1985.

[6] *Guillon, M.*: Hydraulic Servo systems — Analysis and Design. Butterworths, London, 1968.

[7] *Kliffken, M.G.; Kruse, U.*: Robust Control of Electro Hydraulic Actuators in Primar Flight Control. at—Automatisierungstechnik 11/45, 1997.

[8] *Kliffken, M.G.*: Robust Sampled-Data Control of Hydraulic Flight Control Actuators. Fifth Scandinavian International Conference on Fluid Power, Linköping, 1997.

[9] *Kliffken, M.G.*: Nichtlineare strukturelle Regelung, angewandt auf Stellsysteme der Flugsteuerung. Doctorial Thesis, TU Hamburg–Harburg, 1998.

[10] *Kliffken, M.G.; Gojny, M.H.*: Numerical Robust Implementation of Sampled–Data Controllers for Flight Control Actuators. To appear in: at-Automatisierungstechnik, Munich.

[11] *Kammayer, K.D.; Kroschel, K.*: Digitale Signalverarbeitung — Filterung und Spektralanlyse. B.G. Teubner, Stuttgart, 2nd Ed., 1992.

[12] *Middleton, R.H.; Goodwin G.C.*: Digital Control and Estimation – A Unified Approach. Prentice–Hall, Englewood Cliffs, 1990.

[13] *Pallet, E.H.J.; Coyle, S.*: Automatic Flight Control. Blackwell, Oxford, 4th ed., 1993.

[14] *Raymond, E.T.; Chenoweth, C.C.*: Aircraft Flight Control Actuation System Design. SAE, Warrendale, 1993.

ACKNOWLEDGEMENT

The authors thank the *Daimler–Benz Aerospace Airbus GmbH* for promoting and supporting the projects *Oszillation elektrohydraulischer Ruderstellsysteme mit digitaler Abtastung und dynamischen Störlasten* and *Aktuatorregelung in aeroelastischer Umgebung.*